Journal of Asian Earth Sciences 80 (2014) 148–160

Contents lists available at ScienceDirect

Journal of Asian Earth Sciences

journal homepage: www.elsevier.com/locate/jseaes

Late Triassic tuff intervals in the Ordos basin, Central China: Their epositional, petrographic, geochemical characteristics and regional implications

Xinwei Qiu [a,b,*], Chiyang Liu [b,*], Guangzhou Mao [c], Yu Deng [b], Feifei Wang [b], Jianqiang Wang [b]

[a] State Key Laboratory of Isotope Geochemistry, Guangzhou Institute of Geochemistry, Chinese Academy of Sciences, Guangzhou 510640, China
[b] State Key Laboratory of Continental Dynamics, Department of Geology, Northwest University, Xi'an 710069, China
[c] College of Geological Science & Engineering, Shandong University of Science and Technology, Qingdao 266510, China

ARTICLE INFO

Article history:
Received 10 April 2013
Received in revised form 29 October 2013
Accepted 8 November 2013
Available online 20 November 2013

Keywords:
Tuff intervals
Pyroclastic rocks
Event stratigraphy
Late Triassic
Ordos basin
Central China

ABSTRACT

Tuff intervals of Upper Triassic Yanchang Formation are laterally widespread in the Ordos basin, Central China. This paper focuses on magmatic origins and potential source regions of these tuff intervals through detail depositional, petrographic and geochemical analyses. Most of the tuff intervals are well-documented at the bottom of the Chang7 oil reservoir unit and can be correlated laterally, and certain tuff beds are reworked by turbidity current or seismic activity. Petrographic studies of the Chang7 tuffs indicate that they are composed of crystal shards, lithic shards and altered glass shards, and the crystal shards include plagioclase, quartz and biotite. Alteration of the Chang7 tuffs is ubiquitous, thus, most of these tuffs transformed into illite/smectite (I/S) mixed-layers which are identified by scanning electron microscopy (SEM) and X-ray diffraction (XRD). Less common minerals are also detected in the Chang7 tuffs such as zircon, hematite, siderite, anatase. Major elements are determined by the X-ray fluorescence (XRF) analysis, the results indicate that the Chang7 tuffs are enriched in K_2O (average 4.21%), the ratio of SiO_2/Al_2O_3 ranges from 1.73 to 2.85 (average 2.17), and the ratio of TiO_2/Al_2O_3 varies between 0.006 and 0.032 (average 0.017), which imply that the Chang7 tuffs originated from a felsic parental magma. Trace elements are determined by inductively coupled plasma mass spectrometry (ICP-MS), indicating the total rare earth element ($\sum$REE) concentrations are variable, and range from 117.46 to 466.83 ppm (average 251.88 ppm). REE distribution pattern of the Chang7 tuffs presents a LREE rightward incline with flat HREE curve. The value of δEu ranges from 0.151 to 0.837 (average 0.492), suggesting a strong to weak negative Eu anomaly. The Chang7 tuffs show positive anomalies in Rb, Th and U and negative anomalies in Nb, Sr and Eu on a primitive mantle normalized spidergram. A preliminary analysis of the geochemical composition of the Chang7 tuffs suggests a parental magma origin of rhyodacite/dacite, which came from volcanic arc-related setting along an active continental margin. Combined with the chronology and geochemical studies of the synchronous Tianshui rhyolite in the West Qinling Mountains, we propose that the west Qinling Mountains is one of the potential source regions of these tuffs, and the Middle-Late Triassic terminal closure of eastern Tethys provided the arc-related magma.

1. Introduction

Explosive volcanic eruptions can produce large amounts of fine-grained pyroclastic materials which may spread laterally by wind drift over large areas (Kolata et al., 1987; Huff et al., 1992; Königer and Lorenz, 2002; Königer et al., 2002; Huff, 2008). The volcanic ashes are preserved when deposited in marine and nonmarine sedimentary basins, and subsequently altered to clay minerals during diagenetic processes (Huff et al., 2010). However, based on the morphology, composition and mineralogy of unaltered phenocrysts in the volcanic ashes, the magmatic and tectonic setting of the source volcanoes can be inferred (Sharma et al., 2005; Su et al., 2009; Huff et al., 2010; Sell and Samson, 2011). The relatively immobile element compositions of the altered volcanic ashes can also be used to determine the tectonomagmatic setting of the parental magma by applying tectonic and magmatic discrimination diagrams (e.g. Huff et al., 1992; Kramer et al., 2001; Königer and Lorenz, 2002; Foreman et al., 2008; Fanti, 2009).

The Middle-Late Triassic closure of the east Tethys along the Mianlue suture belt was proposed owing to the presence of discontinuous ophiolite suites (Zhang et al., 1996; Lai et al., 1998; Dong et al., 2011), and the diachronous collision between Yangtze and

* Corresponding authors. Tel.: +86 20 85290997 (X. Qiu). Tel.: +86 29 88302352 (C. Liu).
E-mail addresses: qxweilt@126.com (X. Qiu), lcy@nwu.edu.cn (C. Liu).

1367-9120/$ - see front matter © 2013 Elsevier Ltd. All rights reserved.
http://dx.doi.org/10.1016/j.jseaes.2013.11.004

North China blocks from the Late Permian in the east to the Middle-Late Triassic in the west is proposed by various workers (Zhao and Coe, 1987; Yin and Nie, 1993; Zhang et al., 1996; Zhu et al., 1998; He et al., 2007). The collision facilitated the uplift of the Qinling Mountains, and induced the development of synchronous foreland basin in the southwestern Ordos area (Zhang et al., 1996; Liu, 1998; Meng and Zhang, 1999). This mountain building event was recorded by widespread magmatism and metamorphism (Zhang et al., 1996), and a number of syn/post-collisional Indosinian granites have been studied in the west Qinling Mountains by many workers (Sun et al., 2002; Wang et al., 2007; Qin et al., 2008, 2009; Zhu et al., 2011), however, arc-related volcanic rocks of this age are yet to be reported from the area. Fortunately, many contemporaneous Yanchang Formation tuff intervals are preserved in the Ordos basin, especially at the bottom of the Chang7 oil reservoir unit, which represent frequently volcanic eruptions. The Chang7 tuffs can be traced easily due to their logging signatures of high gamma-ray (GR), sonic velocity (AC) and resistivity (R), and low self-potential (SP) (Zhang et al., 2006; Deng et al., 2008; Qiu et al., 2009), and the Chang7 tuffs present positive thorium (Th) anomaly that are revealed by natural gamma spectrometry logging data (Qiu et al., 2010). According to the drill core data and logging signatures, we created a preliminary isopach map of the Chang7 tuffs in the Ordos basin (Fig. 1a, Qiu et al., 2009), which shows clear decrease in the total Chang7 tuffs thickness toward the northeast, indicating that the original volcanic sources must have come from the southwestern part or southern part out of the present Ordos basin. The mineralogical and chemical compositions of the altered Chang7 tuffs tend to be very useful tools for deciphering the tectonomagmatic setting of the potential volcanic sources.

Although the tuff intervals in the Yanchang Formation have been recognized as very useful stratigraphic correlation tools by earlier workers (e.g. Deng et al., 2008; Qiu et al., 2009; Zhang et al., 2009; Li et al., 2009; Zou et al., 2012), their petrographic and geochemical data are limited. In this paper, the depositional, petrographic and geochemical data of the Chang7 tuffs in the Ordos basin is documented. We mainly focus on the tectonomagmatic setting of parental magma, and probe the potential volcanic sources of these tuffs.

2. Geological setting

The Ordos basin is an important nonmarine petroliferous basin, which accounts for about one third of the total oil and gas output of China and has huge resource potential (Yang and Deng, 2013). Mesozoic–Cenozoic Ordos basin developed on the Paleozoic North China craton, on top of a Paleoproterozoic crystalline basement (Wan et al., 2013), which is bounded by poly-phase mountain belts: the east–west trending Yinshan Mountains to the north and Qinling Mountains to the south, the south-north trending Taihang Mountains to the east and western Ordos thrust belts (Liu

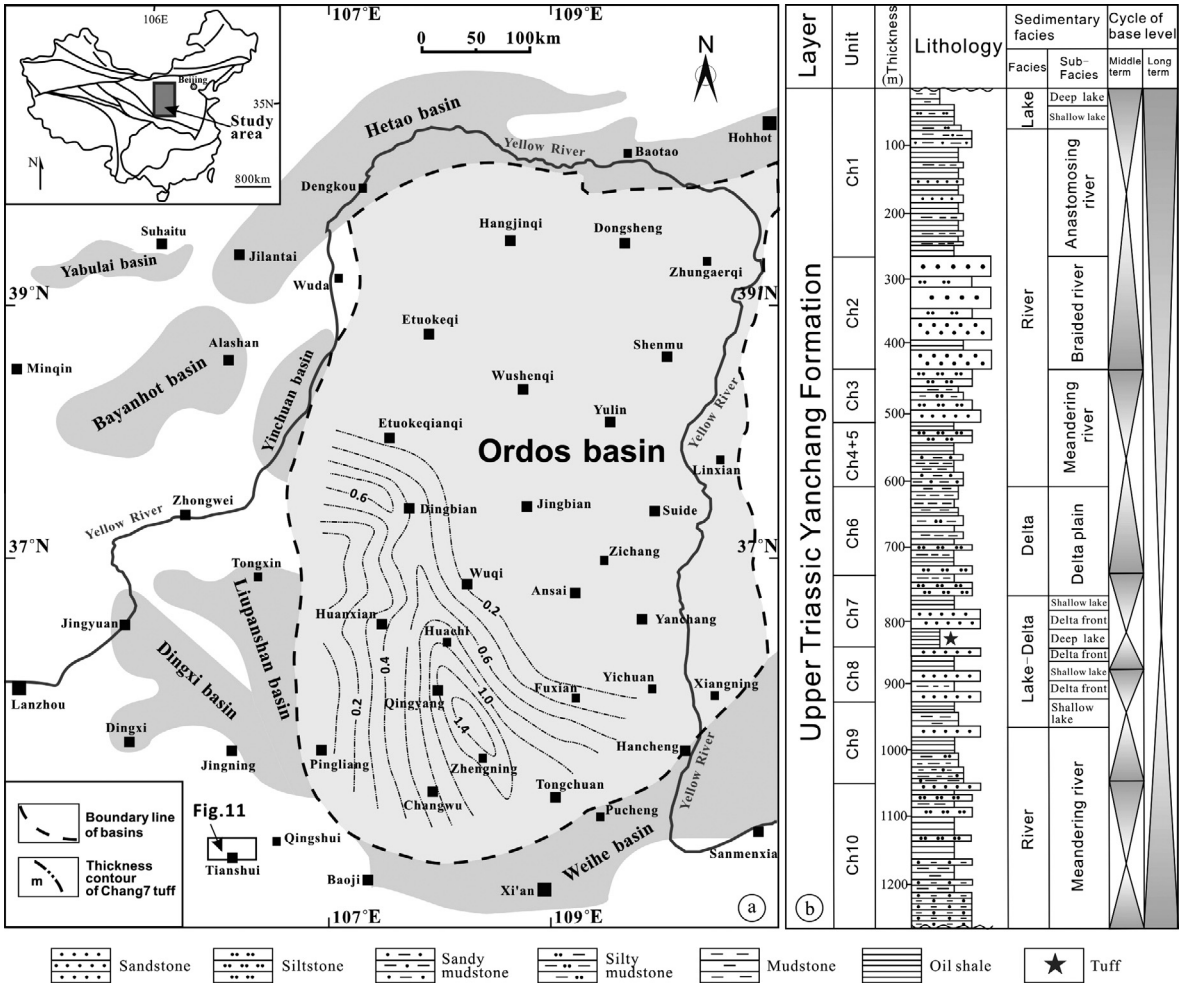

Fig. 1. (a) Isopach map (in meters) of the Chang7 tuff intervals in Ordos basin (after Qiu et al., 2009) and (b) stratigraphic column of Upper Triassic Yanchang Formation in Ordos basin Ch = Chang.

et al., 2008; Johnson and Ritts, 2012). A series of Cenozoic rift basins separate the Ordos basin from adjoining mountains (Fig. 1a). In the Early-Middle Triassic, the area now defined as the Ordos basin was part of the North China intracratonic depression (Liu et al., 2008), and by the Late Triassic the southwestern Ordos basin had evolved as a foreland basin that was characterized in its asymmetric cross-section by low-gradient northeastern and high-gradient southwestern flanks (Liu, 1998; Liu and Yang, 2000). Rapid uplift of the Qinling area was associated with a rapid subsidence of the southern Ordos basin during the Late Triassic, which resulted in molasse deposition with a thickness over 2.8 km that was named as "Kongtongshan" conglomerate (Song et al., 2009). Upper Triassic Yanchang Formation is dominated by alluvial fan, alluvial plain, deltaic, fluvial and lacustrine complexes (Li et al., 2009; Zou et al., 2012), and the Yinshan and Qinling Mountains were thought to be the primary provenances for the Upper Triassic fluvial-deltaic sequences in the Ordos basin (Liu et al., 2008; Zou et al., 2012).

The sedimentary deposit of the Upper Triassic Yanchang Formation comprises sandstones, siltstones, mudstones and tuff intervals with a preserved thickness of about 1000–1300 m (Fig. 1b). For exploration and exploitation purposes, the PetroChina Changqing Oilfield Company subdivided the Yanchang Formation into 10 informal oil reservoir units named Chang10 to Chang1 from the bottom to the top by marker beds, sedimentary cycles or lithological association (Fig. 1b) (Li et al., 2009; Zou et al., 2012), these oil reservoir units are conformity contact with each other. The Chang7 lacustrine black shale is used to be as an important maker bed in the Yanchang Formation due to its logging signatures of high GR and low SP (Fig. 3) (Zhang et al., 2006; Qiu et al., 2009), it ranges in thickness from 30 to 60 meters (m) at the bottom of Chang7 oil reservoir unit, and has been proved to be as dominant high quality hydrocarbon source rock for most of Mesozoic oil–gas reservoirs in the Ordos basin (Zhang et al., 2006; Yang et al., 2010; Ji et al., 2010). Concurrent with the Chang7 black shale is the deposition of many tuff intervals, and the depocenter of the Yanchang period paleo-lake contains tuff intervals with a maximum total thickness which are preserved due to low energy depositional conditions (Deng et al., 2008; Qiu et al., 2009), and the thickness distribution of the Chang7 tuffs tend to be decrease toward northeastern part of the Ordos basin (Fig. 1a), suggesting that the volcanic sources could be near to the Qinling Mountains. Tuff samples for this study are collected from the bottom of the Chang7 oil reservoir unit.

3. Depositional environment of the Chang7 tuffs

Generally, the preservation condition of tuff intervals is strongly influenced by the depositional environment and intrabasinal palaeogeographic framework (Haaland et al., 2000; Königer and Lorenz, 2002; Königer et al., 2002). In nonmarine environment, the highest preservation potential of the tuff intervals occurs in lakes where lack of or only very minor reworking (Königer and Lorenz, 2002), but some tuff intervals are still commonly reworked by turbidity current or seismic activity at numerous localities (Haaland et al., 2000; Grevenitz et al., 2003; Saylor et al., 2005).

The individual beds of the Chang7 tuffs vary in thickness from 0.2 to 45 cm (cm), with tabular geometry in outcrop sections (Fig. 2a–c), which show yellow in color that can be easily distinguished from the siliciclastic "background" sediments. The top and the base of these beds are often mudstone-dominated or capped by black shales (Fig. 2a and b). In drill cores, the

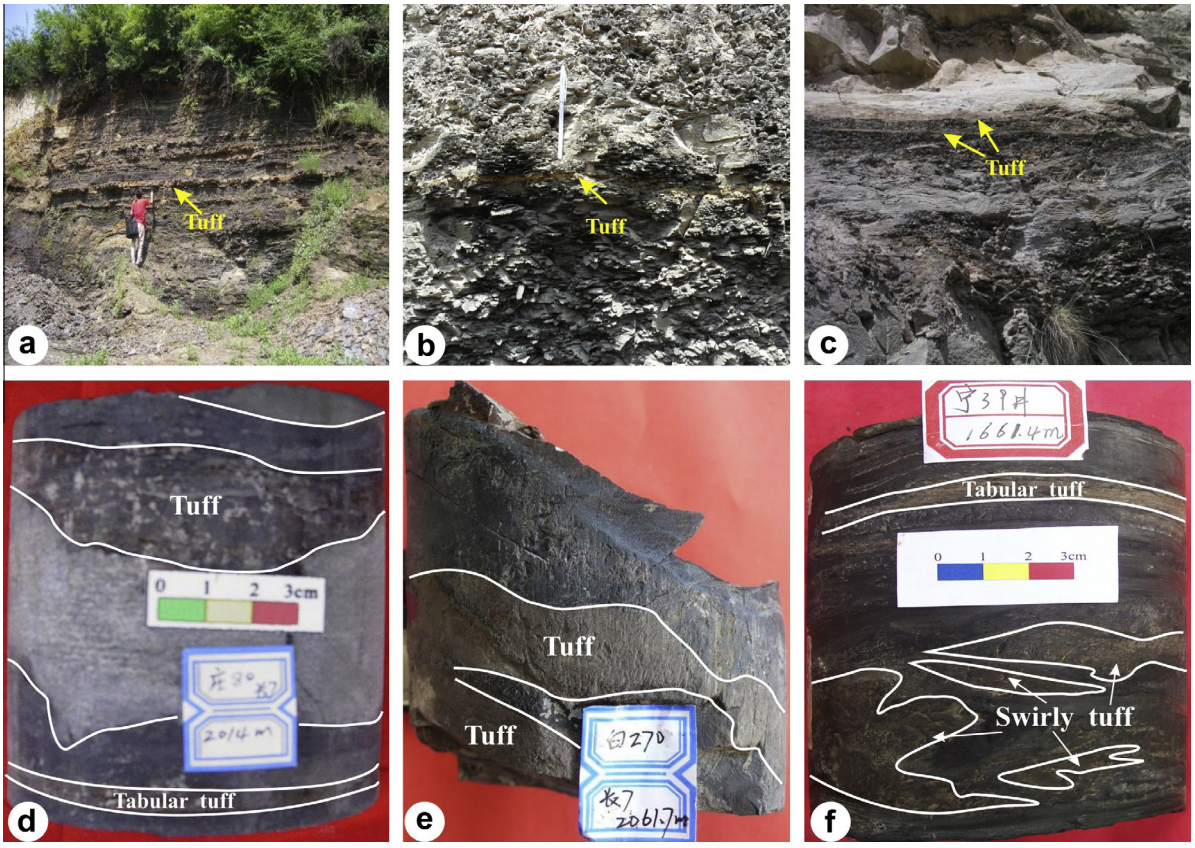

Fig. 2. Chang7 tuff intervals in outcrop sections and cores, (a) Hejiafang section; (b) Shiwanghe section; (c) Yanhe section; (d) Well Zhuang80; (e) Well Bai270 and (f) Well Ning39.

Chang7 tuff intervals show variation in color from yellowish to brown, and most of them are tabular and inter-layered within black shales, which represent wind-transported volcanic ashes deposited in sub-aqueous conditions. Some Chang7 tuff intervals capped with sandstone at the base and black shale on the top, respectively (Fig. 2d), suggesting their association with turbidites. Some deformed tuff intervals associated with black shales have been found (Fig. 2e and f), indicating a local reworking due to slumping or down-slope deposition. Considering the turbidites and seismites have been reported in the Chang7 oil reservoir unit by numerous workers (e.g. Chen et al., 2006; Li et al., 2007; Xia and Tian, 2007; Fu et al., 2008; Yang et al., 2010; Zou et al., 2012; Qiu et al., 2013), we propose that the swirly Chang7 tuff intervals were reworked by the post-depositional turbidity current or seismic activity, thereby stratigraphic correlation of the Chang7 tuff intervals should be attempted with caution due to effects of reworking, an absence of obviously logging signatures in one or several wells represent an absence of tuff intervals or those tuffs have been reworked.

More than 80 tuff beds at the bottom of Chang7 oil reservoir unit of the Well Ning33 drill core are identified, the individual bed ranges in thickness from <1 cm to 40 cm, and has a total thickness of 2–3 m (Fig. 3). Interestingly, the Chang7 tuff intervals are associated with plentiful turbidites that are characterized by incomplete Bouma sequences, and considerable typical seismites that are identified by syn-depositional deformation structures, which coexist in the Chang7 oil reservoir unit of the same well section (Ning 33) (Fig. 3). These features suggest that the event deposition of the unit were facilitated by synchronous volcanic eruptions.

4. Samples and analytical methods

4.1. Samples selection

Petrographic and geochemical analyses have been performed on the Chang7 tuffs which are from drill cores locating at the

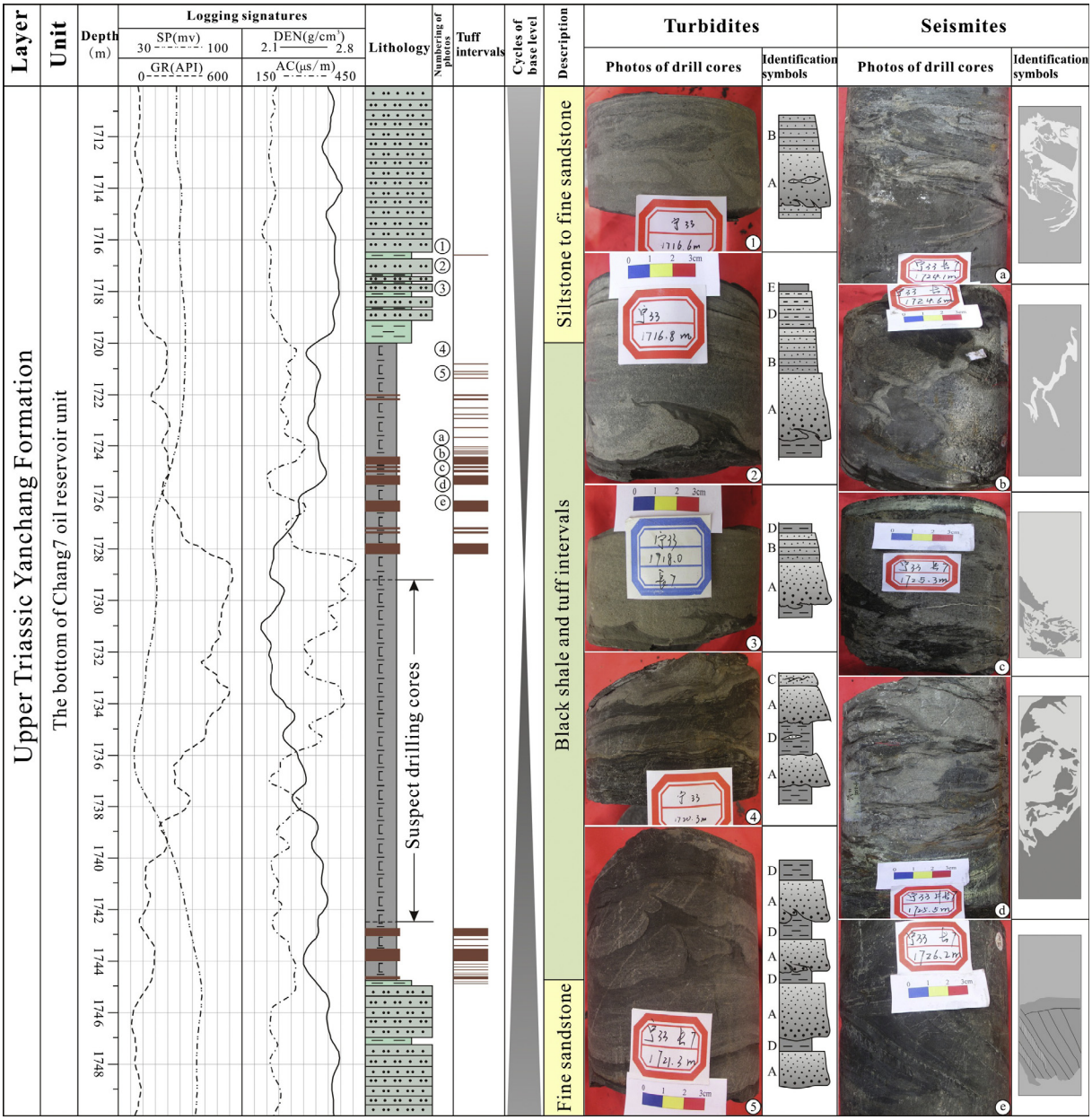

Fig. 3. Tuffs, turbidites and seismites coexist in Chang7 oil reservoir unit of Well Ning33.

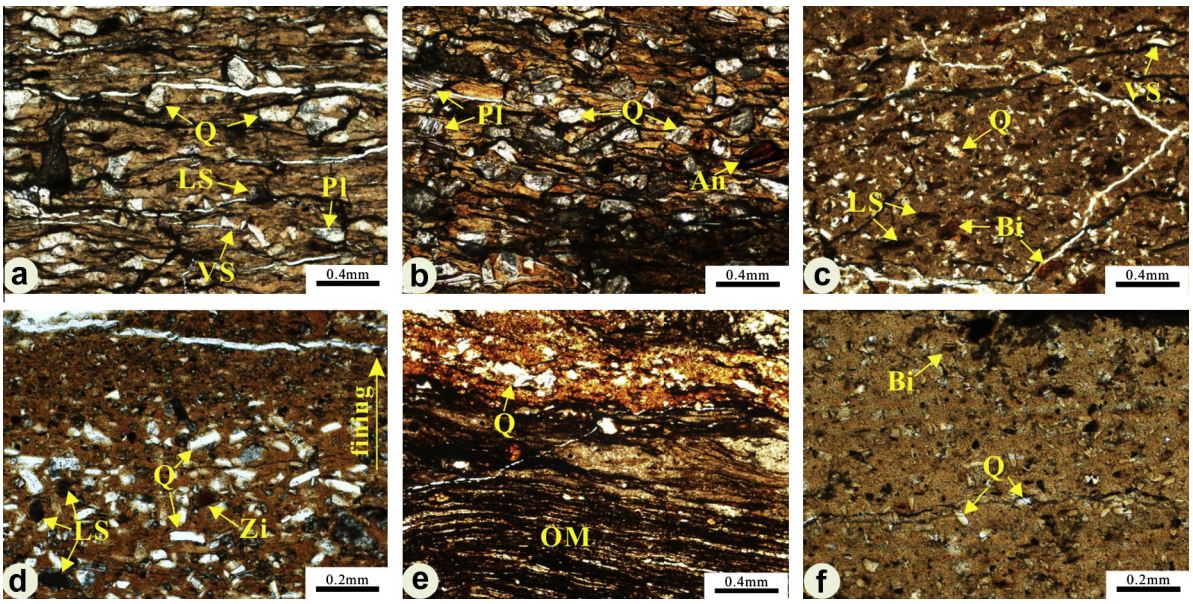

Fig. 4. Characteristics of the Chang 7 tuffs under a single polar microscope, (a) lithic shard, vitric shard and plagioclase in Well Zhuang80; (b) anatase in Well Zhen33; (c) vitric shard and biotite in Well Ning42; (d) zircon in Well Zheng7; (e) organic matter associated with tuffs in Well Zheng11; (f) quartz and biotite in Well Bai270. LS = lithic shard, VS = vitric shards, Q = quartz, Pl = plagioclase, Bi = biotite, Zi = zircon, OM = organic matter, An = anatase.

Table 1
Mineral composition from XRD analysis of the Chang7 tuffs in Ordos basin. Note: samples CT01, CT03, CT10, CT13, CT15 are the same as Table 2.

Sample	Mineral compositions (wt%)
CT01	I/S mixed layer 57; smectite 4; quartz 24; calcite 2; siderite 7; feldspar 4; undetected 2
CT03	I/S mixed layer 67; illite 4; quartz 4; plagioclase 8; calcite 4; hematite 8; undetected 2
CT10	I/S mixed layer 58; smectite 4; quartz 18; plagioclase 18; undetected 2
CT13	I/S mixed layer 89; kaolinite 4; quartz 3; anatase 2; undetected 2
CT15	I/S mixed layer 55; illite 8; kaolinite 6; quartz 4; plagioclase 17; calcite 2; hematite 5; undetected 3

southwestern Ordos basin. Due to the pervasive alteration and some reworking of the tuff intervals, care was taken to samples only tuff with primary fallout characters and samples containing organic matter was avoided.

4.2. Thin section analyses

Tuff samples from drill cores were sent to the Xi'an Institute of Geology and Mineral Resources for making slices, and the thin sections were studied under a microscope by standard techniques to identify the minerals and for modal analyses at the Department of Geology, Northwest University, China.

4.3. XRD and SEM

Pulverized tuff samples of the fraction <2 μm were determined for the total mineral compositions by X-ray diffraction (XRD) at the Xi'an Institute of Geology and Mineral Resources. Small blocks of the Chang7 tuffs were coated with gold and then observed using a scanning electron microscopy (SEM), in order to obtain typical crystal habit data (including that of clay minerals) at the Department of Geology, Northwest University, China.

4.4. Chemical analyses

Fresh tuff and rhyolite samples were powdered to a 200 mesh using a tungsten carbide ball mill at the State Key Laboratory of Continental Dynamics (SKLCD) in Northwest University, China. Major and trace elements of the Chang7 tuffs and rhyolites were

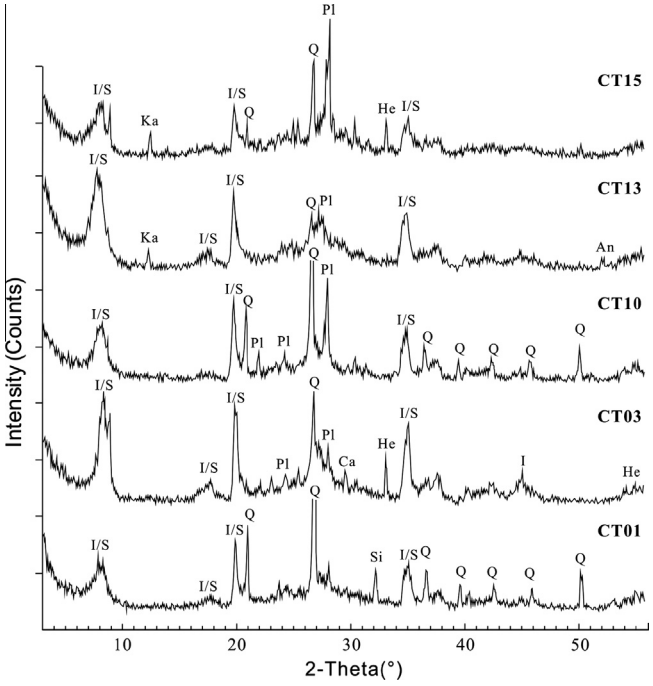

Fig. 5. Representative XRD pattern of the Chang 7 tuffs in Ordos basin, samples CT01, CT03, CT10, CT13, CT15 are the same as Table 2. I/S: illite/smectite; I: illite; Q: quartz; Pl: plagioclase; Ka: kaolinite; He: hematite; Si: siderite; Ca: calcite; An: anatase.

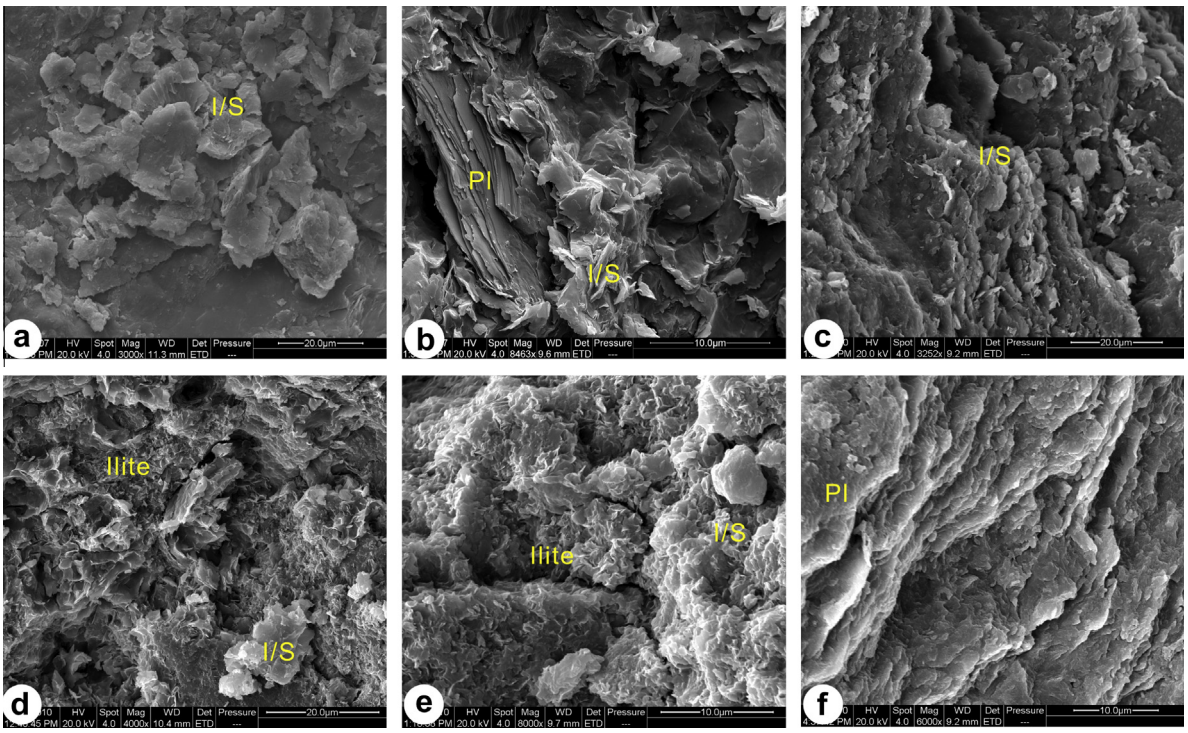

Fig. 6. Clay mineral characteristics of the Chang7 tuffs under a SEM, (a) I/S mixed-layer in Well Zhen59; (b) plagioclase in Well Feng4; (c) I/S mixed-layer in Well Zhuang80; (d) illite in Well Li51; (e) illite in Well Zhen44 and (f) plagioclase in Well Ning33. I/S: illite/smectite; Pl: plagioclase.

determined by XRF (Rikagu RIX 2100) and ICP-MS (Agilent 7500a), respectively. Analyses of International Standards (BHVO-2 and AGV-2) indicate that analytical precision and accuracy for major elements are generally better than 5%. For trace element analysis, sample powders were dissolved using a mixture of HF + HNO_3 in high-pressure Teflon bombs at 190 Celsius degree for 48 h. Analytical precision is better than 5% for the majority of trace elements.

4.5. Zircon U–Pb dating

Rhyolite zircon dating was carried out at the LA-ICP-MS laboratory of the SKLCD. An Agilent 7500a quadruple (Q)-ICPMS instrument was used for simultaneous determination of zircon U–Pb age and trace elements with a 193 nm excimer ArF laser-ablation system attached. The detailed analytical procedure is described in Liu et al. (2010). The $^{206}Pb/^{238}U$ ages were calibrated using zircon 91500 ($^{206}Pb/^{238}U$ age = 1064 Ma; Yuan et al., 2004) as external standard. The fractionation correction and results were calculated using GLITTER 4.0. Subsequently, the method of Andersen (2002) was used to perform common Pb correction. The concordia plot was processed using ISOPOT 3.0 (Ludwig, 2003). The trace element analysis was performed simultaneously with the U–Pb age analysis. Trace element compositions of zircons were calibrated against multiple-reference materials combined with the Si in NIST610 glass as the internal standard (Liu et al., 2010). The accuracy of analyses is better than 10% for the majority of trace elements.

5. Results

5.1. Petrography

The Chang7 tuffs are matrix-supported and mainly consist of crystal, lithic and less altered vitric shards, which are revealed by detailed thin section examination (Fig. 4). The lithic shards are subrounded to subangular ranging in width from 0.02 to 0.5 mm (mm), which are probably derived from pre-existing rocks or incorporated into the tuffs during volcanic eruptions (Fig. 4a, c and d). Sporadic lenses of randomly orientated residual vitric shards occur in the Chang7 tuffs (Fig. 4a and c). The crystal shards are composed by a variety of euhedral to subeuhedral minerals including quartz, plagioclase and biotite, which present well to poorly sorted. The dominantly euhedral quartz grains range in diameter from <0.02 to 0.5 mm, and rarely show undulose extinction (Fig. 4a–c). Rare rounded quartz grains also occur in the Chang7 tuffs, which are probably owing to syn-depositional detrital grains or contamination during local reworking. The angular or elongate plagioclase commonly ranges in length from 0.01 to 0.5 mm, and presents oscillatory zonation (Fig. 4a and b). Zircon and biotite occur as rare (<0.5% modal) accessory minerals (Fig. 4c, d and f). Anatase occurs occasionally in Fig. 4b. Normally graded tuff intervals appear in drill cores, which show gradually fining upward (Fig. 4d). The altered Chang7 tuffs often occur as inter-layer within laminated organic matter (Fig. 4e).

Mineral compositions from XRD analyses are listed in Table 1. Representative XRD diagrams are shown in Fig. 5. The Chang7 tuffs are dominated by clay minerals (61–93%), in which the illite/smectite (I/S) mixed-layer accounts for 55–89%. The amount of quartz varies between 3% and 24% in the Chang7 tuffs. Samples CT03, CT10 and CT15 contain some plagioclase (8–18%). Low content of calcite (2–4%) is detected in samples CT01, CT03 and CT15. Samples CT03 and CT15 contain hematite of 8% and 5%, respectively. Minor siderite (7%) and feldspar (4%) are detected in sample CT01. Sample CT13 has a low content of anatase (2%).

Scanning electron microscope (SEM) reveals a typical I/S mixed-layer texture with curled and lighter edges (Fig. 6a–e), some illites are characterized by a flaky texture (Fig. 6d and e), and plagioclases can be observed in Fig. 6b and f, which confirm that the I/S mixed-layer is dominated in the Chang7 tuffs.

The mineral compositions of the Chang7 tuffs indicate vitric shards of volcanic ash altered extensively into clay minerals that are sensitive to the thermal conditions and geochemical environments (Grevenitz et al., 2003). Some studies revealed that the I/S

mixed-layer in tuffs as well as shale is a diagenetic product of smectite alteration, and the I/S mixed-layer further alter to Chlorite/Smectite (C/S) mixed-layer under a low grade metamorphic condition (Huff et al., 1997). Thus, the high contents of illite-semectite mixed-layer in the Chang 7 tuffs indicate middle to late stages of normal diagenetic alteration without any imprint of low grade metamorphism.

5.2. Major elements

During diagenetic alteration of volcanic ashes, Al_2O_3, CaO, total Fe_2O_3 and P_2O_5 are enriched, whereas SiO_2, Na_2O and K_2O are commonly depleted, concentrations of MgO, MnO and TiO_2 are almost unaffected (Spears and Rice, 1973). In the Chang7 tuff samples, SiO_2 and Al_2O_3 account for about 80% of the total major element content (Table 2). The ratio of SiO_2/Al_2O_3 (weight) ranges from

Table 2
Major (%) and trace (ppm) element data of the Chang7 tuffs in Ordos basin. Note: $\delta Eu = Eu_{CN}/(Sm_{CN} \times Gd_{CN})^{1/2}$; CN = Chondrite Normalized; the normalization value after Sun and McDonough (1989); ∑REE means total rare earth elements.

Sample	CT01	CT02	CT03	CT04	CT05	CT06	CT07	CT08	CT09	CT10	CT11	CT12	CT13	CT14	CT15
Well name	Ning33	Ning33	Zhuang80	Zheng11	Zheng11	Mu9	Bai270	Zhen33	Zhen59	Ning42	Ning42	Ning42	Zhuang210	Xi187	Xi187
Depth (m)	1744.7	1722	2034.5	927	926.5	2311.7	2061.65	2256.7	2460.5	1556.2	1542.4	1557.3	1704.4	2132.8	2132.5
SiO_2	59.81	56.12	51.86	54.11	60.71	53.50	55.29	53.01	55.25	61.93	54.89	58.21	53.57	54.06	55.94
TiO_2	0.29	0.17	0.80	0.27	0.23	0.48	0.17	0.78	0.53	0.29	0.26	0.59	0.44	0.30	0.72
Al_2O_3	20.97	26.24	30.06	27.79	22.44	25.77	28.07	24.14	23.59	21.79	25.58	20.44	27.24	27.59	24.11
TFe_2O_3	3.48	2.69	1.51	2.50	1.74	3.95	1.71	3.72	3.33	2.46	3.02	3.56	2.41	2.46	2.93
MnO	0.03	0.01	0.01	0.01	0.01	0.02	<0.01	0.05	0.02	0.01	<0.01	0.03	0.01	0.01	0.03
MgO	1.77	1.46	1.35	2.04	1.00	1.77	1.12	1.72	1.58	1.61	1.49	2.05	2.15	1.87	1.79
CaO	1.02	0.76	0.70	0.39	1.26	0.48	0.41	2.93	2.84	0.55	0.66	1.64	0.61	0.43	2.48
Na_2O	0.72	1.15	1.00	0.66	1.50	0.89	1.06	2.46	3.10	1.65	1.29	1.38	0.65	1.06	2.15
K_2O	4.00	3.97	5.35	5.61	4.49	3.35	3.40	3.34	3.45	3.82	4.34	4.27	5.38	4.82	3.60
P_2O_5	0.08	0.05	0.13	0.07	0.11	0.19	0.07	0.16	0.14	0.14	0.10	0.15	0.11	0.06	0.11
LOI	7.35	6.99	6.80	6.75	6.03	9.12	8.62	6.98	6.55	5.58	7.92	6.94	6.74	6.85	5.66
Total	99.52	99.61	99.57	100.20	99.52	99.52	99.92	99.29	100.38	99.83	99.55	99.26	99.31	99.51	99.52
SiO_2/Al_2O_3	2.85	2.14	1.73	1.95	2.71	2.08	1.97	2.20	2.34	2.84	2.15	2.85	1.97	1.96	2.32
TiO_2/Al_2O_3	0.0138	0.0065	0.0266	0.0097	0.0102	0.0186	0.0061	0.0323	0.0225	0.0133	0.0102	0.0289	0.0162	0.0109	0.0299
Li	10.9	17.6	13	8.38	25.2	27.2	6.5	35.4	13.6	11.3	14.8	21.9	11.1	12.8	14.8
Be	4.65	4.43	4.95	9.39	8.51	3.31	6.81	3.65	3.69	6.79	6.04	5.29	8.76	5.59	3.8
Sc	6.97	11.6	9.26	8.51	5.55	12.1	4.76	8.21	8.79	5.81	9.36	13.8	9.28	11.5	7.82
V	19.4	24.2	59.2	23.1	20.9	48.8	20.3	46.2	55.1	46.3	35.4	176	29	52.3	46.4
Cr	4.78	13	20.2	5.88	19.9	21.9	3.78	11.4	33	6.65	9.68	32.8	10.2	26.8	14.3
Co	40.5	36.9	6.63	3.47	1.51	14.2	4.28	4.24	12.7	13.1	4.11	26.8	0.87	12.6	3.19
Ni	1.5	8.02	8.12	5.61	8.71	10.1	3.47	5.49	12.9	2.94	6.47	16.5	3.43	15.8	3.21
Cu	8.94	11	17.4	8.04	6.56	30.7	7.58	16.7	23.9	4.63	12.1	23.6	10.7	18.8	13.4
Zn	43.5	103	61.1	75.7	64	166	102	86.9	104	66.3	107	105	53.9	143	70.6
Ga	24.9	29.6	30.2	32.2	30.8	27.1	39.3	28.1	27.9	24.5	32	26.2	35	39.3	27.4
Ge	1.66	1.21	1.21	1.36	1.46	1.79	1.33	1.34	1.73	1.61	1.52	1.94	1.68	1.37	1.44
Rb	143	129	111	180	241	129	113	135	120	153	159	220	169	146	147
Sr	486	219	363	717	186	149	229	709	370	408	252	300	707	656	781
Y	30.4	20.1	24	42.1	48.4	22	44.5	20.8	22.2	25.1	42.5	34.7	46.9	28.1	28.1
Zr	240	183	323	306	208	194	175	283	219	167	323	226	323	202	320
Nb	14.5	11.8	16.5	15.4	17.9	11.6	9.96	13.4	11.9	13.8	21.8	18.9	16	16.3	17.2
Cs	9.64	10.1	9.12	17.5	7.5	7.57	11.7	9.51	7.06	9.3	15	13.7	17.2	11.3	12.4
Ba	963	1393	1295	1447	549	853	763	945	1152	858	895	886	1157	1424	1238
La	57.6	26.6	49.2	25.5	49.3	36.1	80.2	52.5	24.6	66.5	64.7	48.5	99.1	69.6	74.6
Ce	120	57.4	82.1	56.8	98.4	77.6	174	107	47.6	120	136	94	215	157	148
Pr	12.5	6.52	7.33	5.72	10.1	8.54	18.6	10.5	5.32	10.9	14.9	10.1	22.4	16.9	14.8
Nd	45	25.5	24.6	20.2	35.4	32.2	68.2	35.9	19.7	35.9	55.8	36.8	79.9	63.9	51.5
Sm	8.17	5.77	4.35	3.8	7.12	6.58	14.5	6.22	3.9	5.49	11.1	7.04	15.7	12	8.94
Eu	0.66	1.02	0.5	0.75	0.74	0.92	0.8	0.85	0.88	0.88	1.53	1.24	2.37	2.2	1.01
Gd	6.43	4.72	3.43	3.54	6.23	4.92	11.8	4.44	3.41	4.38	9.25	5.87	11.4	7.81	6.55
Tb	1.03	0.74	0.57	0.67	1.09	0.73	1.83	0.65	0.52	0.63	1.46	0.93	1.54	0.95	0.94
Dy	6.03	4.07	3.68	5.02	7	4.08	10.2	3.77	3.3	3.72	8.45	5.64	8.3	4.77	5.35
Ho	1.23	0.77	0.84	1.28	1.58	0.82	1.95	0.77	0.81	0.82	1.69	1.21	1.63	0.92	1.07
Er	3.25	1.88	2.63	4.16	4.73	2.24	4.85	2.15	2.73	2.44	4.43	3.47	4.39	2.36	2.96
Tm	0.47	0.27	0.43	0.69	0.77	0.33	0.64	0.32	0.47	0.4	0.65	0.54	0.63	0.31	0.44
Yb	2.92	1.6	2.9	4.52	5.27	2.09	3.7	2.07	3.65	2.78	4.07	3.65	3.91	1.83	2.82
Lu	0.4	0.22	0.43	0.68	0.78	0.31	0.48	0.31	0.57	0.45	0.57	0.56	0.56	0.26	0.4
Hf	7.4	6.97	9.87	9.2	6.99	6.5	11	7.73	6.14	5.54	10	6.56	9.78	7.39	9.35
Ta	1.95	1.64	2.4	2.57	4.43	1.8	3.9	0.91	1.54	2.58	2.68	2.45	2.39	1.82	1.9
Pb	50	58.4	55.5	50.6	58.5	9.67	81.1	40.2	34.5	52.3	14.2	15.5	56.8	43.2	62.8
Th	51.7	22.4	42.9	47.6	56.3	19.3	57.8	23.6	20.2	47.4	42.1	34.7	53.7	24.8	39.3
U	10.1	6.32	9.04	7.89	16.7	8.04	16.1	6.31	3.67	9.25	13.4	13.6	11.6	7.07	8.29
∑REE	265.69	137.08	182.99	133.33	228.51	177.46	391.75	227.45	117.46	255.29	314.6	219.55	466.83	340.81	319.38
δEu	0.28	0.60	0.40	0.63	0.34	0.49	0.19	0.49	0.74	0.55	0.46	0.59	0.54	0.69	0.40
LREE/HREE	11.21	8.61	11.27	5.48	7.32	10.43	10.05	14.71	6.60	15.34	9.29	9.04	13.43	16.74	14.56
$(La/Yb)_{CN}$	14.15	11.93	12.17	4.05	6.71	12.39	15.55	18.19	4.83	17.16	11.40	9.53	18.18	27.28	18.98
$(La/Sm)_{CN}$	4.55	2.98	7.30	4.33	4.47	3.54	3.57	5.45	4.07	7.82	3.76	4.45	4.07	3.74	5.39
$(Gd/Lu)_{CN}$	1.99	2.65	0.99	0.64	0.99	1.96	3.04	1.77	0.74	1.20	2.01	1.30	2.52	3.71	2.02
Zr/Hf	32.43	26.26	32.73	33.26	29.76	29.85	15.91	36.61	35.67	30.14	32.30	34.45	33.03	27.33	34.22
Nb/Ta	7.44	7.20	6.88	5.99	4.04	6.44	2.55	14.73	7.73	5.35	8.13	7.71	6.69	8.96	9.05

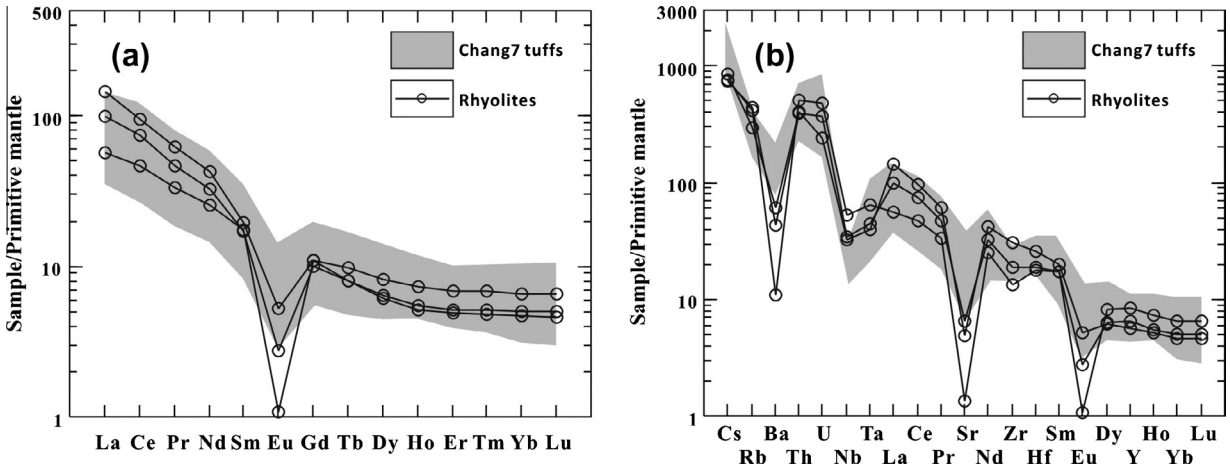

Fig. 7. REE distribution pattern (a) and spidergram (b) of the Chang 7 tuffs and Tianshui rhyolites, the primitive mantle values are from Sun and McDonough (1989).

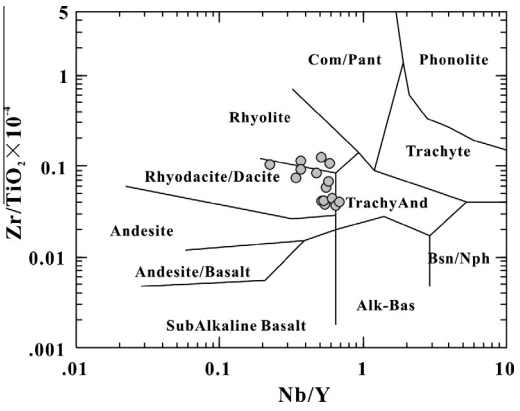

Fig. 8. Zr/TiO_2-Nb/Y discrimination diagram for the Chang7 tuffs (after Winchester and Floyd, 1977).

1.73 to 2.85, with an average of 2.27, which is close to the theoretical value of illite, indicating a relatively pure illite with minor free SiO_2. The ratio of TiO_2/Al_2O_3 (weight) is the most useful indicator for provenance, which is less than 0.02 for typically acidic volcanic rocks (Zhou et al., 2000; Burger et al., 2002). Our data show that the TiO_2/Al_2O_3 ratio ranges from 0.006 to 0.032 with an average of 0.017, which is consistent with an acidic magmatic origin (Table 2). TiO_2 content varies between 0.17% and 0.80% (average 0.42%), and the contents of Fe, Mg, Ca and Mn oxides are relatively low, but the content of K_2O is high, ranging from 3.34% to 5.61% (average 4.21%), which is similar to the typical Paleozoic European K-bentonite (Kolata et al., 1987; Huff et al., 1997; Huff et al., 2010; Su et al., 2009).

5.3. Trace elements

Trace element compositions of the Chang7 tuffs are also given in Table 2. Total rare earth element (∑REE) content ranges from 117.46 to 466.83 ppm, with an average of 251.88 ppm, which is higher than the averages of PAAS (182 ppm) (McLennan, 1989) and NASC (176.2 ppm) (Haskin et al., 1968), respectively. The ratio

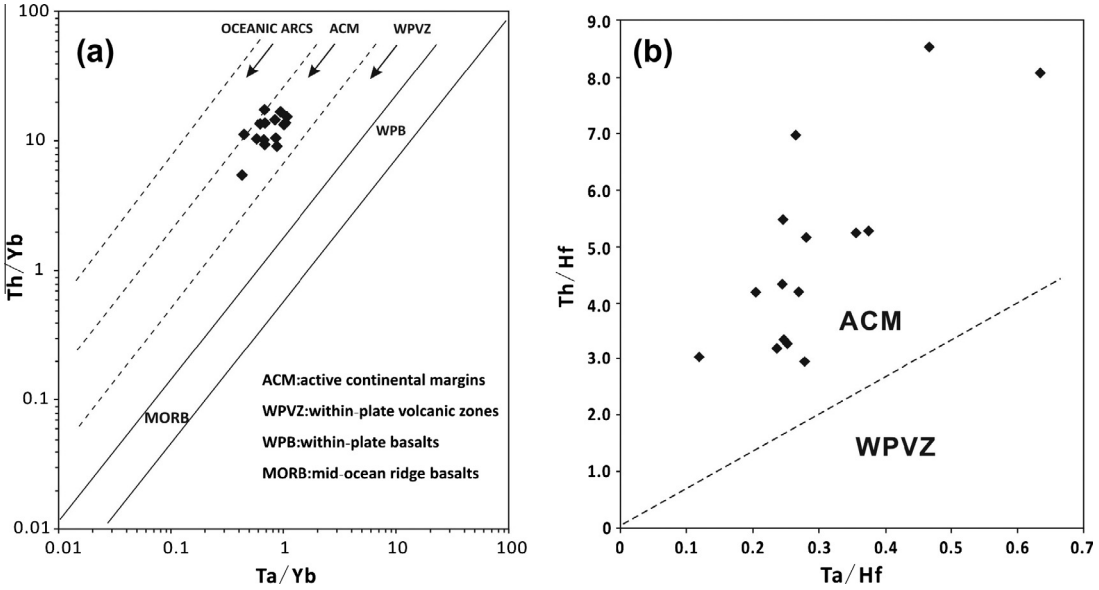

Fig. 9. Discrimination diagrams of Th/Yb versus Ta/Yb (a) (after Gorton and Schandl, 2000) and Th/Hf versus Ta/Hf (b) (after Schandl and Gorton, 2002) for tectonic settings. ACM and WPVZ in (b) are the same as (a).

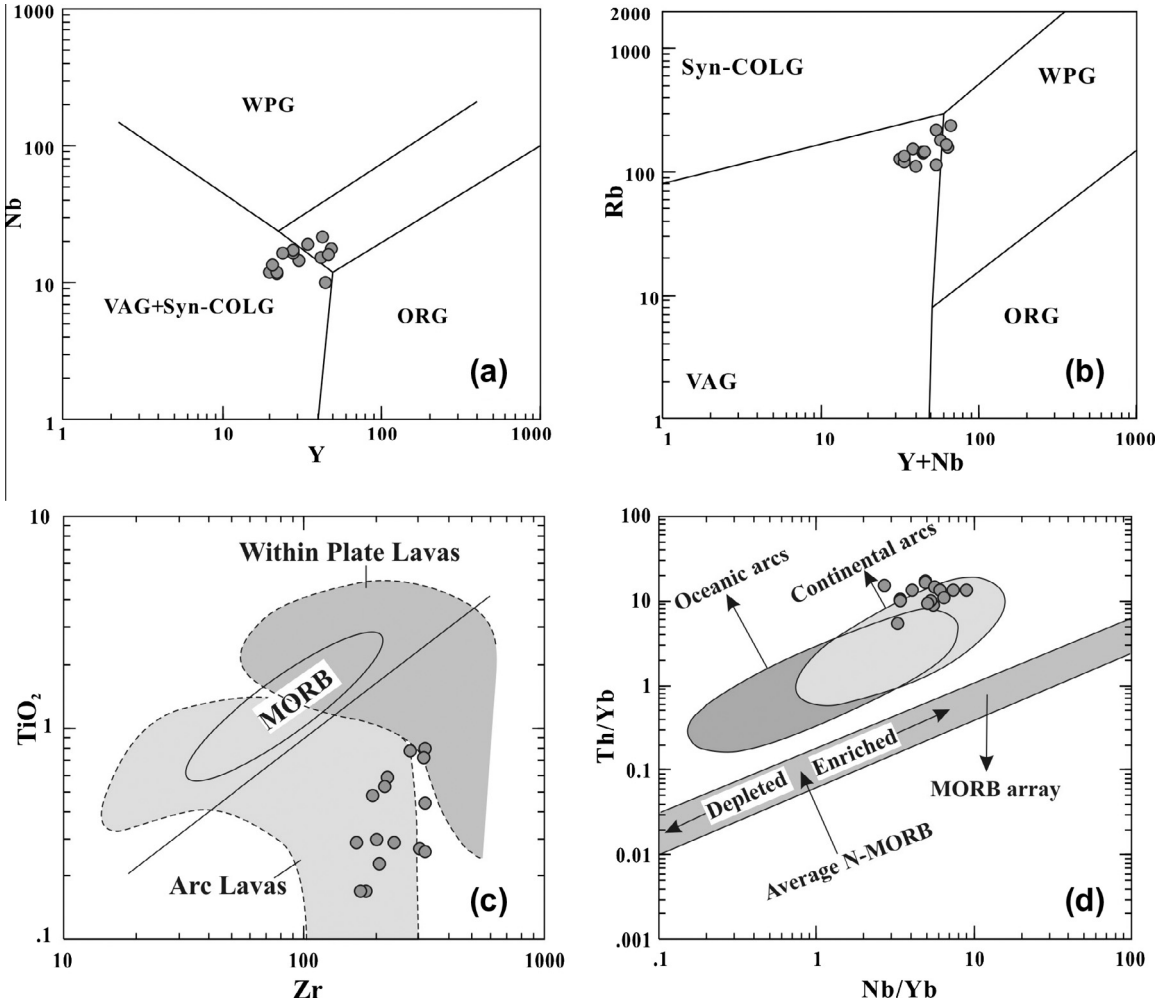

Fig. 10. Tectonic discrimination diagrams for the Chang7 tuffs. (a and b) After Pearce et al., 1984, VAG: volcanic arc granite; Syn-COLG: syn-collisional granite; WPG: within plate granite; ORG: ocean ridge granite; (c) after Pearce, 1982 and (d) after Pearce and Peate, 1995.

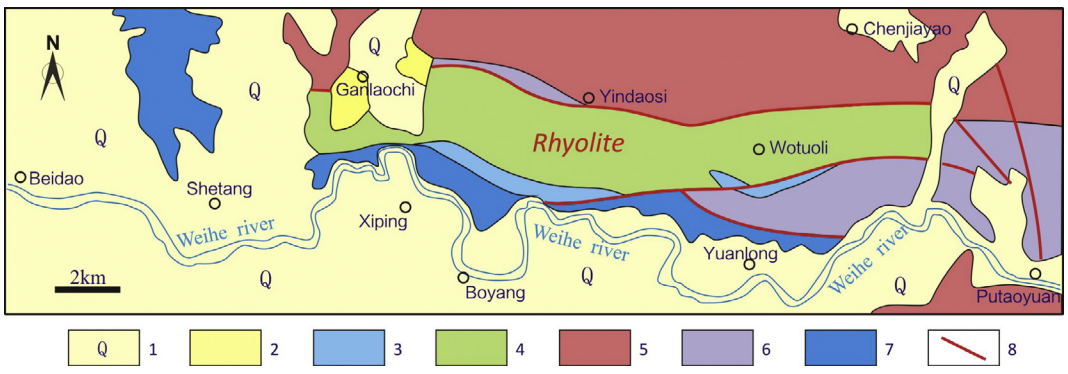

Fig. 11. Simplified geological map of the Tianshui rhyolite in the West Qinling Mountains. 1. Quaternary sediments; 2. Neogene Gansu group; 3. Syenite porphyry; 4. Indosinian rhyolite; 5. Indosinian granite; 6. Early Paleozoic Huluhe group; 7. Proterozoic gneiss and 8. fault.

of LREE/HREE (Light REE/Heavy REE) ranges from 5.48 to 16.74 (average 10.94), and the value of $(La/Yb)_{CN}$ (CN = Chondrite Normalized) varies between 4.05 and 27.28 (average 13.50), indicating the Chang7 tuffs are relatively enriched in the LREE. The mean of $(La/Sm)_{CN}$ (4.63) is higher than the average of $(Gd/Lu)_{CN}$ (1.83), suggesting that the LREEs are more fractionation than HREEs. The Chang7 tuffs show a negative Eu anomaly (δEu = 0.19–0.74), indicating incomplete crystallization of plagioclase was retaining in original magma. REE primitive mantle normalized diagram of the Chang7 tuffs is shown in Fig. 7a, displaying a rightward incline of LREE with flat HREE distributive curve. The evidently negative Eu anomaly and REE distribution pattern suggest the parental magma formed in a subduction-related volcanic arc environment.

The Chang7 tuffs show strong positive anomalies in Rb, Th and U, and negative anomalies in Nb, Sr and Eu on a primitive mantle normalized spidergram (Fig. 7b), which are thought to be related

Table 3
Zircon dating data of the Tianshui rhyolite in the west Qinling Mountains.

Spot	Th	U	Th/U	Pb^{207}/Pb^{206}	±1σ	Pb^{207}/U^{235}	±1σ	Pb^{206}/U^{238}	±1σ	Pb^{208}/Th^{232}	±1σ	Pb^{207}/Pb^{206}	±1σ	Pb^{207}/U^{235}	±1σ	Pb^{206}/U^{238}	±1σ	Pb^{208}/Th^{232}	±1σ
BY01	40.4	51.3	0.79	0.06614	0.00705	0.3111	0.03222	0.03411	0.00095	0.01263	0.00064	810.7	209	275.0	25	216.2	6	253.6	13
BY02	312.6	425.8	0.73	0.05475	0.00151	0.25737	0.00659	0.03409	0.00028	0.04812	0.00036	401.9	60	232.5	5	216.1	2	950.0	7
BY03	107.2	108.4	0.99	0.05674	0.00261	0.26634	0.01175	0.03404	0.00041	0.01138	0.00022	480.7	99	239.8	9	215.8	3	228.7	4
BY04	189.1	186.3	1.01	0.05084	0.00246	0.23776	0.01108	0.03392	0.00042	0.01069	0.00022	233.6	108	216.6	9	215.0	3	214.9	4
BY05	302.6	552.1	0.55	0.05233	0.00099	0.24557	0.0041	0.03403	0.00022	0.01082	0.0001	300.0	43	223.0	3	215.7	1	217.5	2
BY06	51.0	71.7	0.71	0.05477	0.00286	0.25633	0.01292	0.03394	0.00045	0.0112	0.00027	402.9	112	231.7	10	215.2	3	225.1	5
BY07	160.3	195.3	0.82	0.05729	0.00314	0.26661	0.01409	0.03376	0.00048	0.01085	0.00027	502.1	117	240.0	11	214.0	3	218.0	5
BY08	51.8	62.8	0.82	0.04907	0.0037	0.23047	0.01692	0.03407	0.00059	0.0106	0.00034	151.4	168	210.6	14	215.9	4	213.1	7
BY09	123.3	122.7	1.01	0.06506	0.00371	0.30427	0.0167	0.03392	0.00053	0.01203	0.0003	776.4	116	269.7	13	215.1	3	241.6	6
BY10	55.4	66.1	0.84	0.05899	0.0032	0.27626	0.01445	0.03397	0.00049	0.01212	0.00028	566.9	114	247.7	12	215.3	3	243.4	6

to a volcanic arc-related setting (Münker, 1998). The ratio of Zr/Hf ranges from 15.91 to 36.61, with an average of 30.93, which is close to the average of volcanogenic claystones (32.6) that are altered from volcanic ash sediments (Zhang et al., 1997). The ratio of Nb/Ta ranges from 2.55 to 14.73, with an average of 7.26, indicating the parental magma of the Chang7 tuffs is mainly derived from the partial melts of Upper Continental Crust (UCC) (Dostal and Chatterjee, 2000).

6. Discussions

6.1. Tectonomagmatic setting

Previously studies indicate that some elements in altered tuffs tend to be unaffected by weathering and reside in as yet unaltered phenocrysts. Such as TiO_2, the high field strength (HFS) elements (Zr, Nb, Hf, Ta) and the REE are commonly considered to be immobile under the conditions of alteration, weathering, diagenesis and low grade metamorphism (Huff et al., 1997; Königer and Lorenz, 2002), thereby the contents or ratios of these elements are useful indicators for petrogenetic processes, which have been employed to provide information on the magmatic and tectonic origin of those tuffs by numerous workers (Huff et al., 1997; Haaland et al., 2000; Königer et al., 2002; Grevenitz et al., 2003).

Quartz, plagioclase, and less commonly biotite are identified in the Chang7 tuffs by standard analysis technique of thin sections, which suggest that the parental magma prior to eruption had an intermediate-to-felsic series magma. Evidence supporting this interpretation is seen when the data are plotted on the Zr/TiO_2-Nb/Y magmatic discrimination diagram of Winchester and Floyd (1977), which shows that the majority of the Chang7 tuff samples fall at the rhyodacite/dacite field, and minor data fall at rhyolite field (Fig. 8). Fractionated REE patterns with LREE enrichment, flat HREE and negative Eu anomaly of the Chang7 tuffs indicate that they are derived from highly evolved calc-alkaline felsic magmas (e.g. Kramer et al., 2001).

Based on the empirical tectonic discrimination diagrams that are derived from studies of igneous rocks of known origins, we can probe the tectonic settings and general magmatic origins, particularly in cases where other geological evidence is ambiguous (Kramer et al., 2001). To determine the possible tectonic setting of the volcanoes responsible for the widespread distribution of the Chang7 tuffs in the Ordos basin, we plotted the tuffs data on the bivariate plots of Th/Yb versus Ta/Yb (Fig. 9a) (Gorton and Schandl, 2000) and Th/Hf versus Ta/Hf (Fig. 9b) (Schandl and Gorton, 2002), indicating the Chang7 tuffs are derived from an active continental margin setting. In the Nb versus Y (Fig. 10a) and Rb versus Y + Nb (Fig. 10b) plots, which are used for discriminating the tectonic setting of granitic rocks (Pearce et al.,1984), the majority of the Chang7 tuffs data fall at the "volcanic-arc granite" field, suggesting the derivation of the Chang7 tuffs from an arc-related source. However, these diagrams must be interpreted with caution as the compositions of the tuffs may reflect the source geochemical characteristics rather than the tectonic setting (Rollinson, 1993). The diagrams of TiO_2-Zr (Fig. 10c) indicate the Chang7 tuffs are mainly derived from a calc-alkaline arc-related magma. Evidences supporting this interpretation are the REE distribution pattern displaying a negative Eu anomaly and LREE rightward incline with flat HREE curve, and the spidergram showing enrichments in Rb, Th and U and depletions in Nb, Sr and Eu, which are typical characteristics of arc-related magmas (e.g. Brown et al., 1984; Münker, 1998). If it is accepted that the Chang7 tuffs are originated from an arc-related source, are they derived from volcanoes in an island- or continental-arc setting? The diagram of Th/Yb versus Nb/Yb (Fig. 10d) shows that the Chang7 tuffs fall at the continental arc field, indicate a normal calc-alkaline, continental arc-related setting occurred in the Late Triassic near to the Southern Ordos basin.

6.2. Potential source region

Considering the lack of evidence for in situ eruptions in the Ordos basin at the time of the volcanic ashes deposition, the vents are most likely locating outside the basin. The grain size and thickness of altered tuffs are closely related to the duration of eruption, rate of release, residence time in the atmosphere, settling velocity and water depth at the site of deposition (Ledbetter and Sparks, 1979). The maximum grain size of residual phenocrysts in the Chang7 tuffs is less than 0.5–0.6 mm (Fig. 4a and b), and the maximum

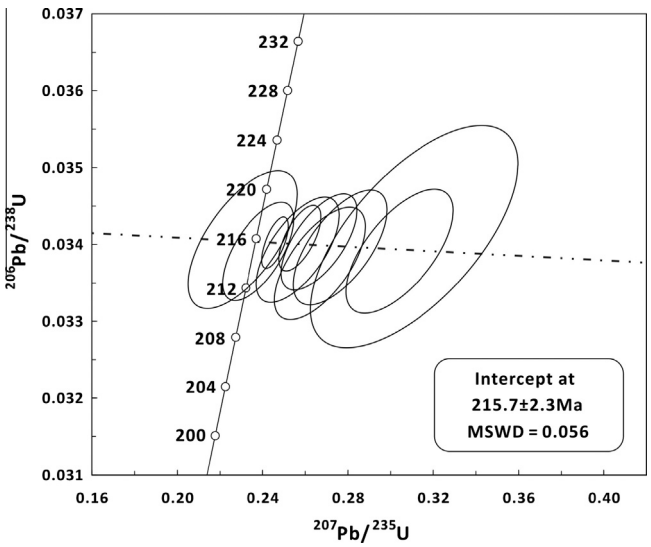

Fig. 12. Zircon U–Pb concordia diagrams of the Tianshui rhyolite.

Table 4
Major (%) and trace (ppm) element data of the Tianshui rhyolites in the west Qinling Mountains. The δEu, CN and ∑REE are the same as Table 2.

Sample	SiO_2	TiO_2	Al_2O_3	TFe_2O_3	MnO	MgO	CaO	Na_2O	K_2O	P_2O_5	LOI	Total	Li	Be	Sc
BY02	71.89	0.14	14.29	2.00	0.09	0.33	0.87	3.57	5.56	0.08	1.26	100.08	20.3	4.10	6.75
BY03	72.48	0.16	13.12	2.46	0.07	1.20	1.21	3.35	5.14	0.06	0.75	100.00	42.6	4.34	9.38
BY04	76.01	0.08	12.60	1.54	0.08	0.26	0.66	3.74	4.61	0.02	0.42	100.02	22.2	6.64	6.95
Sample	V	Cr	Co	Ni	Cu	Zn	Ga	Ge	Rb	Sr	Y	Zr	Nb	Cs	Ba
BY02	8.64	4.94	52.2	1.41	2.15	45.0	18.0	1.63	185.11	104	25.5	338	23.0	6.71	427
BY03	28.7	56.6	44.3	28.2	22.6	41.9	16.8	1.18	277.71	136	29.2	207	24.4	5.85	300
BY04	6.33	9.03	74.8	3.75	3.08	51.8	18.4	1.64	261.32	28.1	37.8	148	37.3	6.01	76.1
Sample	La	Ce	Pr	Nd	Sm	Eu	Gd	Tb	Dy	Ho	Er	Tm	Yb	Lu	Hf
BY02	97.7	168	16.9	57.2	8.68	0.87	6.47	0.86	4.45	0.84	2.34	0.35	2.28	0.34	7.94
BY03	67.3	131	12.8	43.9	7.58	0.46	5.87	0.86	4.68	0.90	2.47	0.38	2.46	0.37	5.82
BY04	38.3	82.1	9.20	34.0	7.72	0.18	6.41	1.06	6.02	1.19	3.25	0.50	3.23	0.48	5.41
Sample	Ta	Pb	Th	U	SiO_2/Al_2O_3	TiO_2/Al_2O_3	∑REE	δEu	δCe	LREE/HREE	$(La/Yb)_{CN}$	$(La/Sm)_{CN}$	$(Gd/Lu)_{CN}$	Zr/Hf	Nb/Ta
BY02	1.64	41.8	34.4	5.02	5.03	0.010	367.70	0.33	0.92	19.50	28.93	7.08	2.32	42.6	14.00
BY03	1.79	34.7	33.3	7.68	5.52	0.012	281.10	0.20	1.01	14.63	18.47	5.58	1.98	35.5	13.64
BY04	2.66	53.5	42.6	9.92	6.03	0.006	193.70	0.07	1.02	7.75	8.00	3.13	1.66	27.4	13.99

thickness of the individual beds is about 40 cm (Fig. 3), which indicate the distance of volcanic source is no more than 200 km that was revealed by the similar volcanic eruption of Mount St. Helens in 1980 (Sarna-Wojcicki et al., 1981). The direction of the Late Triassic paleo-monsoon was mainly from the southwestern part to the northeastern part across the Ordos basin due to the existence of east Tethys (Carroll et al., 2010), and the investigation suggests the clear decrease in total thickness of Chang7 tuff intervals toward the northeastern Ordos basin (Fig. 1a), indicating these tuffs are from the southwestern part or southern part out of the Ordos basin (Fig. 1a). In addition, the grain sizes of residual phenocrysts in the Chang7 tuffs show a decrease in diameter from the southwestern of 0.5–0.6 mm (Fig. 4a and b) to the middle part of 0.1–0.2 mm (Fig. 4c and d), and then to the northeastern of less than 0.1 mm (Fig. 4f). All above facts indicate the volcanic source is most probably located at the west Qinling Mountains that is no more than 200 km out of the Ordos basin.

It is unlikely that volcanoes exist in the northern part and eastern part of this basin, due to lack of a synchronous tectonic event and volcanic eruption to provide these tuffs (Zhang et al., 2002). The Qinling orogenic belt is located at the southern part of the Ordos basin, which has undergone a complex evolution process since Proterozoic, it is widely accepted that the Middle-Late Triassic collision of the South China blocks with the South Qinling orogen along the Mianlue suture belt that led to final integration of the North and South China blocks (Zhang et al., 1996; Meng and Zhang, 1999), and many metavolcanic rocks were well dated showing a range in age from 220 to 245 Ma along this suture belt (Li et al., 1996; Lai et al., 1998), which are slightly older than the deposition age of the Chang7 tuff in the Yanchang Formation, because the flora of *Danaeopsis-Bernoullia* assemblage and the bivalve fauna of *Shaanxiconcha-Unio* assemblage represent the depositional age of the Yanchang Formation is Norian stage (208–227 Ma) (Shannxi BGMR, 1989). Large amounts of contemporaneous magmatic events that was recorded by granitic rocks in the west Qinling Mountains (Wang et al., 2007; Qin et al., 2008, 2009; Jiang et al., 2010; Zhu et al., 2011), and the Chang7 tuffs show a strong compositional affinity with the Late Triassic granites that were thought to be originated from arc-related magmas in the west Qinling Mountain (Jiang et al., 2010). However, these granites are dismissed as possible sources due to those are intrusive rocks. If the volcanic arc related, which represent the widespread magmatic events are attribute to the subduction of Yangtze block beneath into North China block to provide a continental arc-related magma, which imply the terminal closure of the east Tethys produced huge amounts of arc-related volcanic rocks. However, synchronous volcanic rocks were thought to be very limited in the Qinling Mountains (Zhang et al., 2008).

Recently, the synchronous Tianshui rhyolite possessing a 211 Ma U–Pb zircon age was found in the West Qinling Mountains (Fig. 11, Xu et al., 2007), the locality of the rhyolites is no more than 200 km out of the southwestern Ordos basin. This paper dates the rhyolite again by LA-ICP-MS zircon method obtaining a crystallization age of 215.7 ± 2.3 Ma (Table 3 and Fig. 12), that is consistent with the depositional age of the Chang7 tuffs (Shannxi BGMR, 1989) and the preliminary zircon U–Pb age of 205–228 Ma (Zhang et al., 2009; Yang and Deng, 2013). Furthermore, the major and trace element data of these rhyolites are determined to compare with the Chang7 tuffs, the results indicate that the TiO_2/Al_2O_3 ratio of the rhyolites ranges from 0.006 to 0.012, that is similar to the Chang7 tuffs (Table 4). The REE distribution pattern and spidergram of the Tianshui rhyolites present a consistency with the Chang7 tuffs (Fig. 7), thus, the chronology and geochemical data suggest the Tianshui rhyolite might be a possible volcanic source of the Chang7 tuffs. However, more detail investigation is needed to find the consanguinity of these tuffs in future.

7. Conclusions

The tabular Chang7 tuffs present normally graded as inter-layers within black shale, indicating the volcanic ashes deposited in a sub-aqueous environment, certain tuff beds showing disturbed laminations are attribute to the result of reworking by turbidity currents or seismic activity. The tuffs, turbidites and seismites coexist in the Chang7 oil reservoir unit of the same well (Ning33), indicating the turbidity currents and the paleo-earthquakes were activated by adjoining volcanism (e.g. Caddah et al., 1998; Haaland et al., 2000; Grevenitz et al., 2003).

The clay mineral compositions of the Chang7 tuffs consist mainly of I/S mixed-layer. Some residual phenocrysts are identified including quartz, plagioclase, biotite and zircon, which indicate the Chang7 tuffs are mainly derived from felsic series magma. Major and trace element data suggest that the tectonomagmatic origin of the Chang7 tuffs was related to calc-alkaline arc magma which formed in an active continental margin setting. Combined with the distribution pattern, mineralogical, geochemical data of the Chang7 tuffs, and geochemical data of synchronous Tianshui rhyolites, allow us to propose that the rhyolite in the west Qinling Mountains might be a possible volcanic source of the Chang7 tuffs,

which suggest these magmas formed during the northward subduction of Yangtze block beneath into North China block, linked to the terminal closure of the east Tethys.

Acknowledgements

This work was supported by the National Natural Science Foundation of China (Grant Nos. 41203043 and 90814005) and National Science & Technology Major Program of China (Grant No. 2011ZX05001-004). Two anonymous reviewers are thanked for their constructive suggestions to improve this manuscript.

References

Anderson, T., 2002. Correction of common lead in U–Pb analyses that do no report ^{204}Pb. Chemical Geology 192, 59–79.
Brown, G.C., Thorpe, R.S., Webb, P.C., 1984. The geochemical characteristics of granitoids in contrasting arcs and comments on magma sources. Journal of the Geologcial Society 141, 413–426.
Burger, K., Zhou, Y.P., Ren, Y.L., 2002. Petrography and geochemistry of tonsteins from the 4th member of the Upper Triassic Xujiahe formation in southern Sichuan province, China. International Journal of Coal Geology 49, 1–17.
Caddah, L.F.G., Alves, D.B., Mizusaki, A.M.P., 1998. Turbidites associated with bentonites in the Upper Cretaceous of the Campos basin, offshore Brazil. Sedimentary Geology 115, 175–184.
Carroll, A.R., Graham, S.A., Smith, M.E., 2010. Walled sedimentary basins of China. Basin Research 22, 17–32.
Chen, Q.H., Li, W.H., Guo, Y.Q., Liang, J.W., Cui, J.P., Zhang, D.F., 2006. Turbidite systems and the significance of petroleum exploration of Yanchang Formation in the Southern Ordos basin. Acta Geologica Sinica 80 (5), 656–663 (in Chinese with English abstract).
Deng, X.Q., Liu, F.X., Liu, X.Y., Pang, J.L., Lv, J.W., Li, S.X., Liu, X., 2008. Discussion on relationship between sedimentary evolution of the Triassic Yanchang Formation and the Early Indosinian movement in Ordos basin. Journal of Palaeogeography 10 (2), 159–166 (in Chinese with English abstract).
Dong, Y.P., Zhang, G.W., Neubauer, F., Liu, X.M., Genser, J., Hauzenberger, C., 2011. Tectonic evolution of the Qinling orogen, China: review and synthesis. Journal of Asian Earth Sciences 41, 213–237.
Dostal, J., Chatterjee, A.K., 2000. Contrasting behavior of Nb/Ta and Zr/Hf ratios in a peraluminous granitic pluton (Nova Scotia, Canada). Chemical Geology 163, 207–218.
Fanti, F., 2009. Bentonite chemical features as proxy of late Cretaceous provenance changes: a case study from the western Interior basin of Canada. Sedimentary Geology 217, 112–127.
Foreman, B.Z., Rogers, R.R., Deino, A.L., Wirth, K.R., Thole, J.T., 2008. Geochemical characterization of bentonite beds in the two medicine formation (Campanian, Montana), including a new ^{40}Ar/^{39}Ar age. Cretaceous Research 29, 373–385.
Fu, Q., Lv, M.M., Liu, Y.D., 2008. Developmental characteristics of turbidite and its implication on petroleum geology in Late Triassic Ordos basin. Acta Sedmentologica Sinica 26 (2), 186–192 (in Chinese with English abstract).
Gorton, M.P., Schandl, E.S., 2000. From continents to island arcs: a geochemical index of tectonic setting for arc-related and within-plate felsic to intermediate volcanic rocks. The Canadian Mineralogist 38, 1065–1073.
Grevenitz, P., Carr, P., Hutton, A., 2003. Origin, alteration and geochemical correlation of Late Permian airfall tuffs in coal measures, Sydney basin, Australia. International Journal of Coal Geology 55, 27–46.
Haaland, H.J., Furnes, H., Martinsen, O.J., 2000. Palaeogene tuffaceous intervals, Grane Field (Block 25/11), Norwegian North Sea: their depositional, petrographical, geochemical character and regional implications. Marine and Petroleum Geology 17, 101–118.
Haskin, L.A., Haskin, M.A., Frey, F.A., 1968. Relative and absolute terrestrial abundances of the rare earth. In: Ahrens, L.H. (Ed.), Origin and Distribution of the Elements. Pergamon, Oxford, pp. 889–911, vol. 1.
He, D.F., Zhuang, Z.H., Ma, Y.S., 2007. Paleomagnetism characteristics of Triassic in Songpan-Aba block and its kinematic indication. Geoscience 21 (3), 556–563 (in Chinese with English abstract).
Huff, W.D., 2008. Ordovician K-bentonites: issues in interpreting and correlating ancient tephras. Quaternary International 178, 276–287.
Huff, W.D., Bergström, S.M., Kolata, D.R., 1992. Gigantic Ordovician volcanic ash fall in North America and Europe: biological, tectonomagmatic, and event-stratigraphic significance. Geology 20, 875–878.
Huff, W.D., Bergström, S.M., Kolata, D.R., Sun, H.P., 1997. The lower Silurian Osmundsberg K-bentonite Part II: mineralogy, geochemistry, chemostratigraphy and tectonomagmatic significance. Geological Magazine 135 (1), 15–26.
Huff, W.D., Bergström, S.M., Kolata, D.R., 2010. Ordovician explosive volcanism. In: Finney, S.C., Berry, W.B.N. (Eds.), The Ordovician Earth System: Geological Society of America Special Paper, vol. 466, pp. 13–18.
Ji, L.M., Yan, K., Meng, F.W., Zhao, M., 2010. The oleaginous Botryococcus from the Triassic Yanchang Formation in Ordos Basin, Northwestern China: morphology and its paleoenvironmental significance. Journal of Asian Earth Sciences 38, 175–185.
Jiang, Y.H., Jin, G.D., Liao, S.Y., Zhou, Q., Zhao, P., 2010. Geochemical and Sr-Nd-Hf isotopic constraints on the origin of Late Triassic granitoids from the Qinling orogen, Central China: implications for a continental arc to continent-continent collision. Lithos 117, 183–197.
Johnson, C.L., Ritts, B.D., 2012. Plate interior poly-phase basins. In: Busby, C., Azor, A. (Eds.), Tectonics of sedimentary basins: Recent Advances, pp. 567–582.
Kolata, D.R., Frost, J.K., Huff, W.D., 1987. Chemical correlation of K-bentonite beds in the Middle Ordovician Decorah subgroup, upper Mississippi valley. Geology 15, 208–211.
Königer, S., Lorenz, V., 2002. Geochemistry, tectonomagmatic origin and chemical correlation of altered Carboniferous-Permian fallout ash tuffs in southwestern Germany. Geological Magazine 139 (5), 541–558.
Königer, S., Lorenz, V., Stollhofen, H., Armstrong, R.A., 2002. Origin, age and stratigraphic significance of distal fallout ash tuffs from the Carboniferous-Permian continental Saar-Nahe basin (SW Germany). International Journal of Earth Sciences 91 (2), 341–356.
Kramer, W., Weatherall, G., Offler, R., 2001. Origin and correlation of tuffs in the Permian Newcastle and Wollombi coal measures, NSW, Australia, using chemical fingerprinting. International Journal of Coal Geology 47, 115–135.
Lai, S.C., Zhang, G.W., Yang, Y.C., Chen, J.Y., 1998. Geochemistry of the ophiolite and island arc volcanic rock in the Mianxian-Lueyang suture zone, Southern Qinling and their tectonic significance. Geochemica 27, 283–293 (in Chinese with English abstract).
Ledbetter, M.T., Sparks, R.S.T., 1979. Duration of large magnitude explosive eruptions deduced from graded bedding in deep sea ash layer. Geology 7, 40–44.
Li, S.G., Sun, W.D., Zhang, G.W., Chen, J.Y., Yang, Y.C., 1996. Chronology and geochemistry of metavolcanic rocks from Heigouxia Valley in the Mianlve tectonic zone, South Qinling: Evidence for a Paleozoic oceanic basin and its close time. Science in China (Series D) 39, 300–310.
Li, Y.H., Liu, C.Y., Wang, X.J., Guo, Z.Q., 2007. Characteristics and geological significance of sandstone dikes in the Triassic Yanchang Formation of the Ordos basin. Geology in China 34 (3), 400–405 (in Chinese with English abstract).
Li, W.H., Pang, J.G., Cao, H.X., Xiao, L., Wang, R.G., 2009. Depositional system and paleogeographic evolution of the late Triassic Yanchang stage in Ordos basin. Journal of Northwest University 39 (3), 501–506 (in Chinese with English abstract).
Liu, S.F., 1998. The coupling mechanism of basin and orogen in the western Ordos basin and adjacent regions of China. Journal of Asian Earth Sciences 16 (4), 369–383.
Liu, S., Yang, S., 2000. Upper Triassic-Jurassic sequence stratigraphy and its structural controls in the western Ordos basin, China. Basin Research 12, 1–18.
Liu, C.Y., Zhao, H.G., Zhao, J.F., Wang, J.Q., Zhang, D.D., Yang, M.H., 2008. Temporo-spatial coordinates of evolution of the Ordso basin and its mineralization response. Acta Geologica Sinica 82 (6), 1229–1243.
Liu, Y., Gao, S., Hu, Z., Cao, C., Zong, K., 2010. Continental and oceanic crust recycling induced melt-peridotite interactions in the Tran-North China Orogen: U–Pb dating, Hf isotopes and trace elements in zircons of mantle xenoliths. Journal of Petrology 51 (1–2), 537–571.
Ludwig, K.R., 2003. User's manual for Isoplot 3.00: a geochronological toolkit for Microsoft excel. Berkeley Geochronology Center Special, Publication No. 4.
McLennan, S.M., 1989. Rare earth elements in sedimentary rocks: influence of provenance and sedimentary processes. Reviews in Mineralogy and Geochemistry 21, 169–200.
Meng, Q.R., Zhang, G.W., 1999. Timing of collision of the North and South China blocks: controversy and reconciliation. Geology 27, 123–126.
Münker, 1998. Nb/Ta fractionation in a Cambrian arc/back arc system, New Zealand: source constraints and application of refined ICPMS techniques. Chemical Geology 144, 23–45.
Pearce, J.A., 1982. Trace element characteristics of lavas from destructive plate boundaries. In: Thorpe, R.S. (Ed.), Andesits. Wiley, Chichester, pp. 525–548.
Pearce, J.A., Peate, D.W., 1995. Tectonic implications of the composition of volcanic arcmagmas. Annual Review of Earth and Planetary Sciences 23, 251–285.
Pearce, J.A., Harris, N., Tindle, A., 1984. Trace element discrimination diagrams for the tectonic interpretation of granite rocks. Journal of Petrology 15, 956–983.
Qin, J.F., Lai, S.C., Li, Y.F., 2008. Slab break off model for the Triassic post-collisional adakitic granitoids in the Qinling orogenic belt, Central China: zircon U–Pb ages, geochemistry and Sr–Nd–Pb isotopic constraints. International Geology Review 50, 1080–1104.
Qin, J.F., Lai, S.C., Rodney, G., Diwu, C.R., Ju, Y.J., Li, Y.F., 2009. Geochemical evidence for origin of magma mixing for the Triassic monzonitic granite and its enclaves at Mishuling in the Qinling orogen (Central China). Lithos 112, 259–276.
Qiu, X.W., Liu, C.Y., Li, Y.H., Mao, G.Z., Wang, J.Q., 2009. Distribution characteristics and geological significances of tuff interlayers in Yanchang formation of Ordos basin, China. Acta Sedimentologica Sinica 27 (5), 1138–1146 (in Chinese with English abstract).
Qiu, X.W., Liu, C.Y., Mao, G.Z., Deng, Y., Wang, F.F., 2010. Enrichment feature of thorium element in tuff interlayers of Upper Triassic Yanchang formation in Ordos basin, China. Geological Bulletin of China 29 (8), 1185–1191 (in Chinese with English abstract).
Qiu, X.W., Liu, C.Y., Wang, J.Q., Deng, Y., Wang, F.F., Mao, G.Z., 2013. Triggers and characteristics of late Triassic deep-lacustrine synsedimentary deformation

structures in Ordso basin. Chinese Journal of Geology 48 (1), 204–216 (in Chinese with English abstract).
Rollinson, H.R., 1993. Using geochemical data: evaluation, presentation, interpretation. Longman Group UK, 1–315.
Sarna-Wojcicki, A.M., Shipley, S., Waitt, R.B., Dzurisin, D., Wood, S.H., 1981. Areal distribution, thickness, mass, volume, and grain size of air-fall ash from the six major eruptions of 1980. Geological Survey Professional Paper 1250, 577–600.
Saylor, B.Z., Poling, J.M., Huff, W.D., 2005. Stratigraphic and chemical correlation of volcanic ash beds in the terminal Proterozoic Nama group, Namibia. Geological Magazine 142 (5), 519–538.
Schandl, E.S., Gorton, M.P., 2002. Application of high field strength elements to discriminate tectonic settings in VMS environments. Economic Geology 97, 629–642.
Sell, B.K., Samson, S.D., 2011. Apatite phenocrysts compositions demonstrate a miscorrelation between the Millbrig and Kinnekulle K-bentonites of North America and Scandinavia. Geology 39 (4), 303–306.
Shannxi, BGMR (Bureau of Geology and Mineral Resources of Shannxi Province), 1989. In: Regional Geology of the Shannxi Province. Geological Publishing House, Beijing, pp. 1–692 (in Chinese with English abstract).
Sharma, S., Dix, G.R., Villeneuve, M., 2005. Petrology and potential tectonic significance of a K-bentonite in a Taconian shale basin (eastern Ontario, Canada), northern Appalachians. Geological Magazine 142 (2), 145–158.
Song, L.J., Zhao, J.Z., Yuan, B.Q., Liu, C.Y., Wu, C.L., 2009. Development and genetic mechanism of the Kongtongshan Formation conglomerate. Geotectonica et Metallogenia 33 (4), 508–519 (in Chinese with English abstract).
Spears, D.A., Rice, C.M., 1973. An upper Carboniferous tonstein of volcanic origin. Sedimentology 20, 281–294.
Su, W.B., Huff, W.D., Ettensohn, F.R., Liu, X.M., Zhang, J.E., Li, Z.M., 2009. K-Bentonite, black-shale and flysch successions at the Ordovician-Silurian transitions, South China: Possible sedimentary responses to the accretion of Cathaysia to the Yangtze block and its implications for the evolution of Gondwana. Gondwana Research 15, 111–130.
Sun, S.S., McDonough, W.F., 1989. Chemical and isotopic systematics of oceanic basalts: implications for mantle composition and process From. In: Saunders, A.D., Norry, M.J. (Eds.), Magmatism in the Ocean Basins. Geological Society Special Publication, pp. 313–345, vol. 42.
Sun, W.D., Li, S.G., Chen, Y.D., Li, Y.J., 2002. Timing of synorogenic granitoids in the South Qinling, central China: Constraints on the evolution of the Qinling-Dabie orogenic belt. Journal of Geology 110, 457–468.
Wan, Y.S., Xie, H.Q., Yang, H., Wang, A.J., Liu, D.Y., Kröner, A., Wilde, S.A., Geng, Y.S., Sun, L.Y., Ma, M.Z., Liu, S.J., Dong, C.Y., Du, L.L., 2013. Is the Ordos block Archean or Paleoproterozoic in age? Implications for the Precambrian evolution of the North China craton. American Journal of Science 313, 683–711.
Wang, X.X., Wang, T., Jahn, B.M., Hu, N.G., Chen, W., 2007. Tectonic significance of Late Triassic post-collisional lamprophyre dykes from the Qinling Mountains (China). Geological Magazine 144 (5), 837–848.
Winchester, J.A., Floyd, P.A., 1977. Geochemical discrimination of different magma series and their differentiation products using immobile elements. Chemical Geology 20, 325–343.
Xia, Q.S., Tian, J.C., 2007. Characteristics and geological significance of seismites of the Yanchang Formation, Upper Triassic, Ordos basin. Acta Sedmentologica Sinica 25 (2), 246–252 (in Chinese with English abstract).
Xu, X.Y., Wang, H.L., Chen, J.L., Su, X.H., Wu, P., Gao, T., 2007. Zircon U–Pb age, element geochemistry of Mesozoic acid volcanic rocks at Yindaoshi area in western Qinling. Acta Petrologcia Sinica 23 (11), 2845–2856.
Yang, H., Deng, X.Q., 2013. Deposition of Yanchang formation deep-water sandstone under the control of tectonic events, Ordos basin. Petroleum Exploration and Development 40 (5), 513–520 (in Chinese with English abstract).
Yang, H., Zhang, W.Z., Wu, K., Li, S.P., Peng, P.A., Qin, Y., 2010. Uranium enrichment in lacustrine oil source rocks of the Chang 7 member of the Yanchang Formation, Ordos basin, China. Journal of Asian Earth Sciences 29, 285–293.
Yin, A., Nie, S.Y., 1993. An indentation model for the north and south China collision and the development of the Tan-lu and Honam fault systems, eastern Asia. Tectonics 12 (4), 801–813.
Yuan, H.L., Gao, S., Liu, X.M., Li, H.M., Günther, D., Wu, F.Y., 2004. Accurate U–Pb age and trace element determinations of zircon by laser ablation-inductively coupled plasma mass spectrometry. Geoanalytical and Geostandard Research 28 (3), 353–370.
Zhang, G.W., Meng, Q.R., Yu, Z.P., Sun, Y., Zhou, D.W., Guo, A.L., 1996. Orogenesis and dynamics of the Qinling Orogen. Science in China (Ser. D) 39 (3), 225–234.
Zhang, J.M., Li, G.X., Zhou, C.M., 1997. Deposits of volcanic eruption event from the basal Lower Cambrian phosphatic sequence in eastern Yunnan and their significance. Journal of Stratigraphy 21 (2), 91–99 (in Chinese with English abstract).
Zhang, G.W., Dong, Y.P., Pei, X.Z., Yao, A.P., 2002. On the Meso-Cenozoic circum-Siberian intracontinental tectonic system. Geological Bulletin of China 21 (4–5), 198–201 (in Chinese with English abstract).
Zhang, W.Z., Yang, H., Li, J.F., Ma, J., 2006. Leading effect of high-class source rock of Chang 7 in Ordos basin on enrichment of low permeability oil-gas accumulation. Petroleum Exploration and Development 33 (3), 289–293 (in Chinese with English abstract).
Zhang, C.L., Wang, T., Wang, X.X., 2008. Origin and tectonic setting of the Early Mesozoic granitoids in Qinling orogenic belt. Geological Journal of China Universities 14 (3), 304–316.
Zhang, W.Z., Yang, H., Peng, P.A., Yang, Y.H., Zhang, H., Shi, X.H., 2009. The influence of Late Triassic volcanism on the development of Chang7 high grade hydrocarbon source rock in Ordos basin. Geochimica 38 (6), 573–582 (in Chinese with English abstract).
Zhao, X.X., Coe, R.S., 1987. Palaeomagnetic constrainst on the collision and rotation of North and South China. Nature 327 (14), 141–144.
Zhou, Y.P., Bohor, B.F., Ren, Y.L., 2000. Trace element geochemistry of altered volcanic ash layer (tosteins) in Late Permian coal-bearing formations of eastern Yunnan and western Guizhou Province, China. International Journal of Coal Geology 44, 305–324.
Zhu, R.X., Yang, Z.Y., Wu, H.N., 1998. Phanerozoic palaeomagnetic apparent polar wander path and block motion of Chinese primary block. Science in China Series D: Earth Science 28 (Suppl), 1–16.
Zhu, L.M., Zhang, G.W., Chen, Y.J., Ding, Z.J., Guo, B., Wang, F., Lee, B., 2011. U–Pb ages and geochemistry of the Wenquan Mo-bearing granitioids in Western Qinling, China: Constraints on the geodynamic setting for the newly discovered Wenquan Mo deposit. Ore Geology Reviews 39, 46–62.
Zou, C.N., Wang, L., Li, Y., Tao, S.Z., Hou, L.H., 2012. Deep-lacustrine transformation of sandy debrites into turbidites, Upper Triassic, Central China. Sedimentary Geology 265–266, 143–155.